Appl. Phys. A 79, 421–424 (2004)
DOI: 10.1007/s00339-004-2738-3

Applied Physics A
Materials Science & Processing

S.J. LIMMER
S.V. CRUZ
G.Z. CAO✉

Films and nanorods of transparent conducting oxide ITO by a citric acid sol route

University of Washington, Department of Materials Science and Engineering, 302 Roberts Hall, Box 352120, Seattle, WA 98195, USA

Received: 20 February 2004/Accepted: 24 February 2004
Published online: 1 April 2004 •

ABSTRACT We report the synthesis of nanorods of Sn-doped In_2O_3 (ITO) through sol electrophoresis with a template. A citric acid-based sol was developed for the formation. This technique enables the synthesis of ITO nanorods with controlled size and Sn-doping concentration. The nanorods synthesized have diameters of $\sim$ 75–145 nm and show a bulk resistivity of $\sim 5\,\Omega$ cm.

PACS 61.46.+w; 73.63.Bd

1 Introduction

The class of materials known as transparent conducting oxides (TCOs) has become widely used in a number of applications, due to their unique combination of high electrical conductivity and optical transparency. Applications of TCOs are numerous, and include organic light-emitting diodes [1], electrochromic displays [2] and photovoltaic cells [3]. Perhaps the most well-known and widely used TCO material is tin-doped indium oxide (ITO), which has been in use for over 20 years [4]

As the size of devices continues to shrink, the potential application of one-dimensional nanostructures of functional oxides is ever increasing [5]. One can imagine that many current applications for TCOs could be enhanced by the formation of TCO nanorods, along with many potential new applications. In contrast to the numerous reports on the synthesis of metal and semiconductor nanowires [6], there has been little work done in the synthesis of ITO nanorods. A few research groups have reported the formation of undoped In_2O_3 nanowires by oxidation of In nanowires [7], through vapor methods [8] (including thermal evaporation [9, 10] and a vapor–liquid–solid (VLS) technique [11, 12]), or with sol–gel template filling [13] (for hollow ITO nanotubes). However, all of these techniques have drawbacks, and in every case the finished product does not contain the desired Sn doping that gives ITO its high electrical conductivity [14]. One group has reported the synthesis of ITO nanofibers by a VLS technique [15], but there was no mention of the Sn dopant concentration, nor does this technique seem to allow one to control the Sn concentration. In this communication, we report the formation of ITO nanorods with a controlled diameter and Sn dopant concentration through the technique of sol electrophoresis.

2 Experimental

2.1 *Sol preparation*

The chemicals used in making the sols were: indium (III) chloride and tin (IV) chloride (both Alfa Aesar), citric acid monohydrate (Fisher), ethylene glycol (J.T. Baker), absolute ethanol (AAPER) and de-ionized water. Two types of template membranes were used for the growth of the nanorods, namely track-etched hydrophilic polycarbonate (PC) (Millipore Isopore) and anodic alumina (AAM) (Whatman Anodisc). The PC membranes have pore diameters of 100 and 200 nm and a thickness of 10 μm; the AAM samples have 200-nm pores and a thickness of 60 μm.

A citric acid-based ITO sol was developed for the technique. This was necessary because existing sol recipes (such as that by Alam and Cameron [16]) did not result in the formation of nanorods. This method is derived from the ethylene glycol thermal decomposition method of Yamamoto and Sasamoto [17] and the colloidal sol of Stoica et al. [18]. Briefly, the technique consists of the following. First, citric acid monohydrate is dissolved in a mixture of 3 parts ethanol and 2 parts ethylene glycol at 40 °C. The quantity of citric acid is such that the ratio of citric acid : (In + Sn) = 2 : 1. The desired amount of $SnCl_4$ is then added to the solution under stirring. A Sn concentration of 10 at % was chosen to give good electrical conductivity, as reported by Alam and Cameron [16]. Then, $InCl_3$ is added to the solution, and this mixture is stirred for an additional 90 min. During the final half of this time, water is added to complete the hydrolysis of the precursors. The ratio of water : (In + Sn) is 3.1 : 1, including the water of hydration in the citric acid. At the end of the stirring, the sol is cooled to room temperature and vacuum filtered with $\sim$ 1-μm filter paper. The final concentration of ITO in the sol is about 0.12 M.

2.2 *Film preparation*

To test the properties of the sol, thin films were prepared on glass

✉ Fax: +1-206/543-3100, E-mail: gzcao@u.washington.edu

slides by spin coating. First, a thin silica buffer layer was spun on, using a polymeric silica sol [19], to minimize diffusion of Na from the glass into the film [20]. The final ITO film consists of five coats, with a two-step drying (110 and 300 °C) between coats. The films were then given a final firing at 400–700 °C for 1 h in air. Powders were also made by drying the sol at 300 °C and then firing under the same conditions as for the films. X-ray diffraction (XRD) of the powders was done on a Phillips 1830 diffractometer. The film transmission was measured with an Ocean Optics PC2000 spectrometer and the sheet resistance of the films was measured with a Veeco four-point probe. This was converted to a bulk resistivity value by multiplying by the film thickness (~ 550 nm), which was determined by observing a cross section in a JEOL JSM-5200 scanning electron microscope (SEM).

2.3 *Nanorod preparation*

Synthesis of the ITO nanorods was achieved through sol electrophoresis with a template, following the procedure we have outlined previously [21]. Briefly, the PC or AAM template is placed against a working electrode, in contact with the sol. A Pt counter-electrode is placed opposite the working electrode at a distance of ~ 3 cm. Nanorods are grown under an applied potential of 4 V. To verify the importance of the electrophoresis, samples were also synthesized without an applied field, by simply immersing the template in the sol for 1 h. After growth, samples are dried at ~ 110 °C and then fired in air at 600–700 °C for 1 h. The as-synthesized nanorods were observed by SEM (JEOL-JSM 5200 and 820A), transmission electron microscopy (TEM, Phillips EM420T) and energy-dispersive spectroscopy (EDS, Princeton Gamma Tech IMIX). The resistivity of the ITO nanorods was determined with an LCR meter (HP 4284A).

3 Results and discussion

3.1 *Sol*

Most ITO sol recipes reported in the literature require the use of stabilizing additives for the formation of a stable sol. Such additives, typically acetylacetone (AcAc) [16, 22, 23], diethanolamine (DEA) [24] or triethanolamine (TEA) [24, 25], strongly retard the condensation reactions in sols. While this is important for the formation of stable sols, it may be very detrimental to the synthesis of nanorods by sol electrophoretic deposition (EPD). If condensation reactions between deposited nanoclusters do not occur, the nanorod deposit will have no green strength, and will not hold its shape upon pyrolysis of the PC template. If condensation reactions are even further inhibited, nanocluster formation may not even occur in the sol, in which case sol EPD would not be possible.

For this reason, it was necessary to develop a new ITO sol recipe that would work with the sol EPD technique. Citric acid-based sol methods are widely known [26] to be useful for formation of stable complex oxide sols. However, this technique has not been widely adapted for the synthesis of ITO sols, although a paper from Stoica et al. [18] does briefly mention addition of a polybasic acid to their sol. This may have been citric acid, but it is unclear. From our previous research, we have shown that a citric acid-based sol ($Sr_2Nb_2O_7$) can be used for the formation of nanorods [21]. We have adapted this method to the formation of ITO sols with a Sn concentration of about 10%.

3.2 *Films*

First, it was necessary to determine if the new sol produces the desired ITO phase. Powder XRD, shown in Fig. 1, demonstrates that the desired phase has already appeared after heating to 400 °C, with the crystallinity improving upon further heating to 700 °C. Only peaks corresponding to the desired cubic In_2O_3 phase were observed. All fired films are transparent, with a transmission greater than 80% for 450–750 nm (not shown). The films are all conductive as well, with a resistivity dependent on the firing temperature, as seen in Fig. 2. The samples fired at 700 °C have the best properties, with a resistivity of $\sim 1.44 \times 10^{-2}\,\Omega\,\mathrm{cm}$. This value falls roughly in the middle of the range reported in the literature ($\sim 1.5 \times 10^{-3}\,\Omega\,\mathrm{cm}$ [16] to $\sim 2.0 \times 10^{-2}\,\Omega\,\mathrm{cm}$ [27]) for sol–gel ITO films fired in air.

3.3 *Nanorods*

Figure 3 shows SEM micrographs of ITO nanorods grown in 100-nm (A) and 200-nm (B) PC templates and fired at 600 °C for 1 h. These samples show about 25%–30% shrinkage in diameter compared to the original template diameter. The nanorods synthesized in this study are not straight, with a number of the nanorods being

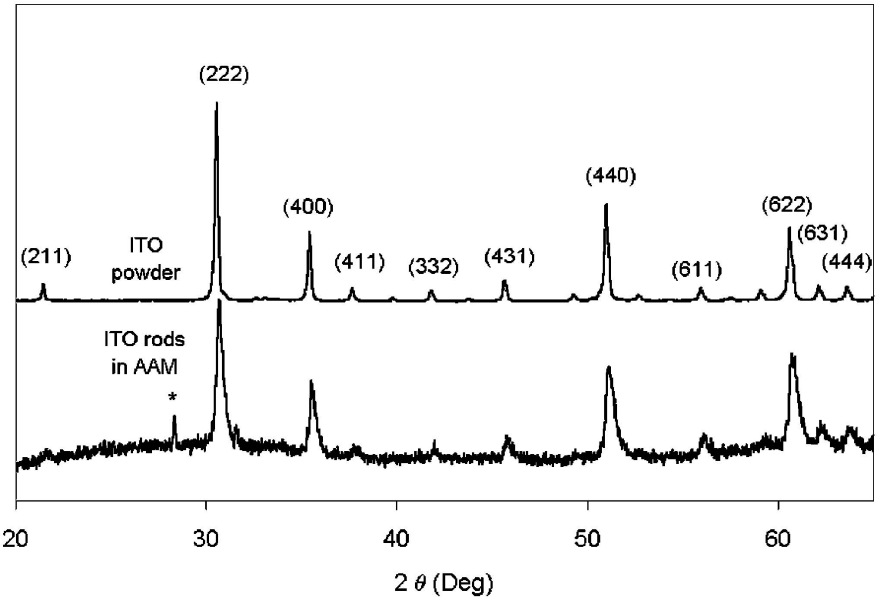

FIGURE 1 XRD patterns for ITO powders and nanorods (in AAM) fired in air at 700 °C for 1 h. The peak marked * does not belong to ITO, or any tin or indium oxides, but may be from the alumina template

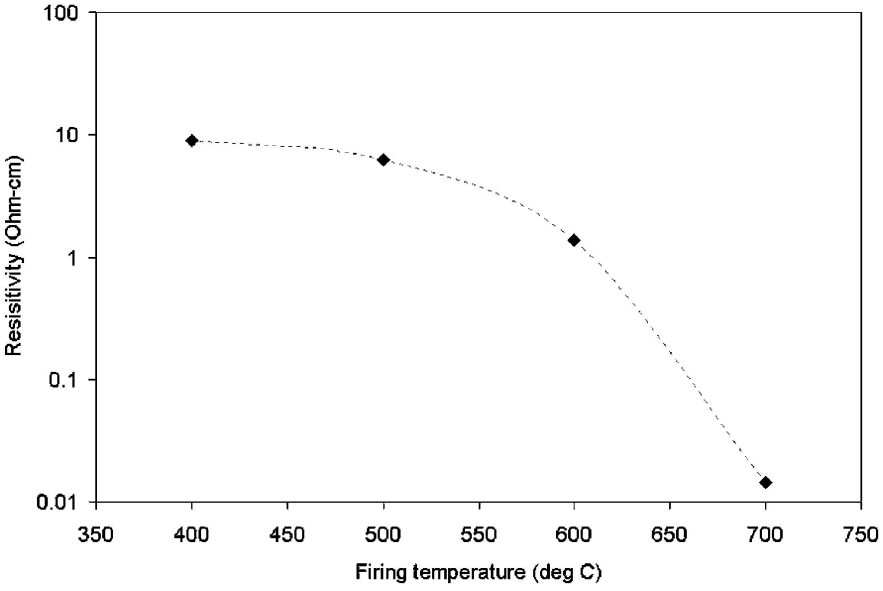

FIGURE 2 Resistivity of ITO films as a function of firing temperature

bent into quite curvy shapes. One possible explanation for this is the drying step used prior to firing. It is believed that this step promotes further surface-condensation reactions between the deposited nanoparticles, and is thus an important part of the nanorod synthesis. This can be seen, for example, in the growth of TiO_2 nanorods in 50-nm templates, where the morphology changes between samples dried for ~ 24 (discontinuous) and ~ 48 h (continuous) at 110 °C [28]. It is thus possible that a further drying time (or increase in drying temperature) could further the surface condensation, and thus yield straighter rods.

To understand the importance of EPD in the growth of the ITO nanorods, samples were also prepared without electrophoresis, by simply immersing the template into the sol for the growth time of 1 h. Figure 3c shows a SEM micrograph of such a sample. It can be seen in this image that the result of the growth without EPD is a low yield of short, broken, hollow nanorods. This is expected, given the expected mechanism of growth when using sol EPD [21].

Figure 4a shows a bright-field TEM micrograph of a single ITO nanorod. From this image, one can see that the nanorod has a mostly smooth surface, but that there are some small fluctuations on the sides of the rod. The selected-area diffraction pattern (Fig. 4b) of one nanorod shows a ring pattern typical of a polycrystalline nanorod. A dark-field TEM image (Fig. 4c) shows the presence of very small crystallites ~ 2–5 nm in size. This is somewhat smaller than the grain sizes determined from XRD line broadening, which show an average crystallite size of ~ 25 nm in the nanorods. This is not surprising, as ITO has been found with a 'grain–subgrain structure', where the smaller subgrains are about 20 times smaller than the grains. XRD line broadening is also of limited accuracy for very fine-grained compacts due to the presence of non-uniform strains [29]. Figure 4d shows the recorded EDS data from a single nanorod. Both the In (24.14 keV) and the Sn (25.20 keV) K_α lines [30] are clearly present, with an intensity ratio that suggests ~ 8 at. % Sn in the In_2O_3. Sn is present in the nanorods, showing that we have successfully produced the desired, doped phase of ITO.

To determine the approximate resistivity of the ITO nanorods, samples were grown in an AAM template for 6 h and then dried. Since a temperature of 700 °C was determined to give the best properties in films, the samples in AAMs were also fired at 700 °C for 1 h. This yields a composite of ITO nanorods embedded in the AAM membrane. The existence of the desired phase is demonstrated in the XRD data shown in Fig. 1, which compares the spectra of ITO powders from this sol (fired at 700 °C) to the nanorods in an AAM. Electrodes were placed on each side of the composite membrane using silver paste and wires were attached. The resistance of this setup was then measured and found to be 2.61 Ω after subtracting the contribution from the wires and the silver electrodes. This data was used to calculate an approximate resistivity for the nanorods, based on the electrode area ($\sim 0.08\ cm^2$), the number density of the nanorods ($10^9\ cm^2$) and the length and diameter of the nanorods (60 μm and ~ 140 nm, respectively). This gives a value of $\sim 5\ \Omega$ cm for the bulk resistivity of the nanorods. Obviously, this

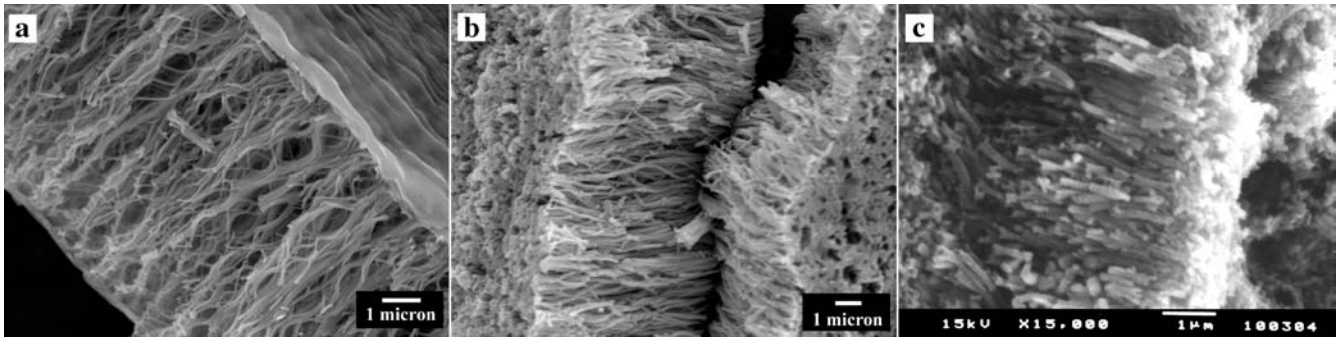

FIGURE 3 SEM micrographs of nanorods of ITO grown in 100-nm (**a**) and 200-nm (**b**) templates. **c** SEM micrograph of a sample where EPD was not used, showing poor-quality nanorods

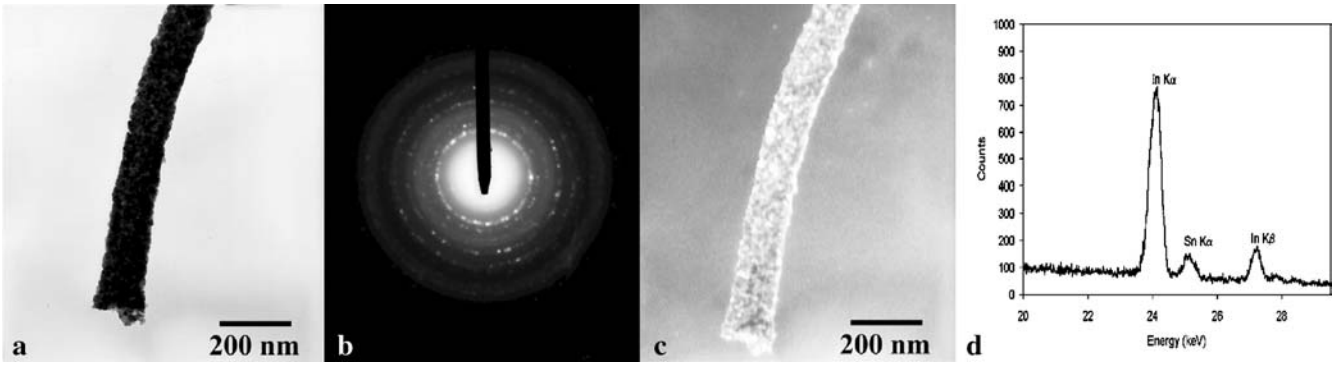

FIGURE 4 **a** Bright-field TEM micrograph of a single ITO nanorod. **b** Electron-diffraction pattern from that rod. **c** Dark-field TEM micrograph, demonstrating the small crystallite size. **d** EDS spectrum of a single ITO nanorod

is a very crude method to determine the resistivity of the nanorods, which is, in part, why the value obtained is so much larger than those typically reported in the literature.

One possible explanation for the large resistivity recorded would be scattering at the grain boundaries or nanorod walls. Using a typical value of the carrier concentration ($n \approx 10^{20}\,\mathrm{cm}^2$) [14] and the resistivity measured from ITO films (of the same sol), one can calculate an electron mean free path of about 3 nm [31]. Thus, grain-boundary scattering may have a detrimental effect on the nanorod resistivity. Additionally, very poor conductivity ($\varrho \approx 800\,\Omega\,\mathrm{cm}$) has been found previously in mesoporous ITO [32]. It is suggested that the low conductivity is due to residual organic components, grain-boundary effects in the powder and defects in the wall structure. It is also possible that not all of the ITO nanorods embedded in the template contribute to the electrical conductivity. Figure 3 suggest that a certain fraction of the ITO nanorods break during or after firing. The additional constraints imposed when sintering samples in the rigid AAM template may lead to an even greater number of broken ITO nanorods. Furthermore, it is possible that not all channels of the AAM are filled, or run through the entire thickness of the template, leading to additional increases in the measured resistivity.

4 Conclusions

Sol electrophoretic deposition in templates is a highly flexible method for the synthesis of a wide variety of nanorods. For example, the technique can be used to synthesize nanorods of the transparent conducting oxide material ITO, which was shown to have an apparent resistivity of 5 Ω cm.

ACKNOWLEDGEMENTS S.J.L. would like to acknowledge financial support from a NSF-IGERT fellowship from the Center for Nanotechnology at the University of Washington.

REFERENCES

1 Y.H. Tak, K.B. Kim, H.G. Park, K.H. Lee, J.R. Lee: Thin Solid Films **411**, 12 (2002)
2 N. Ozer, F. Tepehan, N. Bozkurt: Thin Solid Films **219**, 193 (1992)
3 E. Stathous, P. Lianos, U.L. Stangar, B. Orel: Adv. Mater. **14**, 354 (2002)
4 J.C. Manifacier: Thin Solid Films **90**, 297 (1982)
5 G.R. Patzke, F. Krumeich, R. Nesper: Angew. Chem. Int. Ed. **41**, 2446 (2002)
6 A. Huczko: Appl. Phys. A **70**, 365 (2000)
7 M. Zheng, L. Zhang, X. Zhang, J. Zhang, G. Li: Chem. Phys. Lett. **334**, 298 (2001)
8 L. Dai, X.L. Chen, J.K. Jian, M. He, T. Zhou, B.Q. Hu: Appl. Phys. A **75**, 687 (2002)
9 Z.W. Pan, Z.R. Dai, Z.L. Wang: Science **291**, 1947 (2001)
10 X.S. Peng, Y.W. Wang, J. Zhang, X.F. Wang, L.X. Zhao, G.W. Meng, L.D. Zhang: Appl. Phys. A **74**, 437 (2002)
11 J. Zhang, X. Qing, F. Jiang, Z. Dai: Chem. Phys. Lett. **371**, 311 (2000)
12 C. Li, D. Zhang, S. Han, X. Liu, T. Tang, C. Zhou: Adv. Mater. **15**, 143 (2003)
13 B. Cheng, E.T. Samulski: J. Mater. Chem. **11**, 2901 (2001)
14 R.B.H. Tahar, T. Ban, Y. Ohya, Y. Takahashi: J. Appl. Phys. **83**, 2631 (1998)
15 X.S. Peng, G.W. Meng, X.F. Wang, Y.W. Wang, J. Zhang, X. Liu, L.D. Zhang: Chem. Mater. **14**, 4490 (2003)
16 M.J. Alam, D.C. Cameron: Thin Solid Films **377–378**, 455 (2000)
17 O. Yamamoto, T. Sasamoto: J. Mater. Res. **7**, 2488 (1992)
18 T.F. Stoica, T.A. Stoica, V. Vanca, E. Lakatos, M. Zaharescu: Thin Solid Films **348**, 273 (1999)
19 C.M. Chan, G.Z. Cao, H. Fong, M. Sarikaya: J. Mater. Res. **15**, 148 (2000)
20 F.U. Guanghui, D.U. Jiafeng, P.A.N. Donghui, H.E. Ouli: J. Non-Cryst. Solids **112**, 454 (1989)
21 S.J. Limmer, S. Seraji, Y. Wu, T.P. Chou, C. Nguyen, G.Z. Cao: Adv. Funct. Mater. **12**, 59 (2002)
22 S.R. Ramanan: Thin Solid Films **389**, 207 (2001)
23 H. Tomonaga, T. Morimoto: Thin Solid Films **392**, 243 (2001)
24 J. Liu, E. Rädlein, G.H. Frischat: Phys. Chem. Glasses **40**, 277 (1999)
25 S.-S. Kim, S.-Y. Choi, C.-G. Park, H.-W. Jin: Thin Solid Films **347**, 155 (1999)
26 D. Segal: J. Mater. Chem. **7**, 1297 (1997)
27 D. Yu, W. Yu, D. Wang, Y. Qian: Thin Solid Films **419**, 166 (2002)
28 S.J. Limmer, G.Z. Cao: Adv. Mater. **15**, 427 (2003)
29 B.D. Cullity: *Elements of X-Ray Diffraction*, 2nd edn. (Addison-Wesley, Reading, MA 1978) p. 285
30 L.C. Feldman, J.W. Mayer: *Fundamentals of Surface and Thin Film Analysis* (Elsevier, New York 1986)
31 R.B.H. Tahar, T. Ban, Y. Ohya, Y. Takahashi: J. Appl. Phys. **83**, 2139 (1998)
32 T.T. Emons, J. Li, L.F. Nazar: J. Am. Chem. Soc. **124**, 8516 (2002)